IMPROVEMENT OF MICROPHYSICAL PARAMETERIZATION THROUGH OBSERVATIONAL VERIFICATION EXPERIMENT

BY MARK T. STOELINGA, PETER V. HOBBS, CLIFFORD F. MASS, JOHN D. LOCATELLI, BRIAN A. COLLE, ROBERT A. HOUZE JR., ARTHUR L. RANGNO, NICHOLAS A. BOND, BRADLEY F. SMULL, ROY M. RASMUSSEN, GREGORY THOMPSON, AND BRADLEY R. COLMAN

Improvements in the representation of cloud and precipitation processes in mesoscale models are sought through comparisons of detailed field measurements with model outputs.

Regional mesoscale models are becoming increasingly important for the short-term (0–48 h) operational forecasting of local weather systems and precipitation. However, despite significant improvements in the forecasting of many meteorological parameters, progress in quantitative precipitation forecasting (QPF) over the past several decades has been relatively modest (Olson et al. 1995; Fritsch et al. 1998). Furthermore, as model resolution has increased, problems with model simulations of cloud and precipitation fields have become increasingly apparent (Colle et al. 1999; Colle and Mass 2000; Colle et al. 2000). There are many aspects of an operational numerical weather prediction system that can contribute to errors in QPF: lack of sufficient initial data, deficiencies in data assimilation techniques, insufficient model resolution, numerical errors, and problems with parameterizations of boundary layer processes, convection, and bulk cloud and precipitation microphysics. In high-resolution models, bulk microphysical parameterization (BMP) schemes play a particularly important role in the model-produced QPF. However, comprehensive data needed to verify the physical processes and hydrometeor fields simulated

AFFILIATIONS: STOELINGA, HOBBS, MASS, LOCATELLI, HOUZE, AND RANGNO—Department of Atmospheric Sciences, University of Washington, Seattle, Washington; COLLE—Institute for Terrestrial and Planetary Atmospheres, State University of New York at Stony Brook, Stony Brook, New York; BOND—Department of Atmospheric Sciences, and Joint Institute for the Study of the Atmosphere and Ocean, University of Washington, Seattle, Washington; SMULL—Department of Atmospheric Sciences, University of Washington, Seattle, Washington, and NOAA/National Severe Storms Laboratory, Norman, Oklahoma; RASMUSSEN AND THOMPSON—Research Applications Program, National Center for Atmospheric Research, Boulder, Colorado; COLMAN—National Weather Service, Seattle, Washington
CORRESPONDING AUTHOR: Prof. Peter V. Hobbs, Dept. of Atmospheric Sciences, University of Washington, Box 351640, Seattle, WA 98195-1640
E-mail: phobbs@atmos.washington.edu
DOI: 10.1175/BAMS-84-12-1807

In final form 22 April 2003

by BMP schemes, and to isolate errors in BMP schemes from other sources of error, have not been available. To help fill this need, we have embarked on a study titled the Improvement of Microphysical Parameterization through Observational Verification Experiment (IMPROVE) to compare representations of cloud and precipitation processes in current mesoscale models with detailed observations in a variety of weather systems, with the goal of improving QPF produced by mesoscale models. In this paper we summarize the scientific background for IMPROVE, describe the design and operation of two IMPROVE field campaigns, present some examples of the data obtained, and outline the direction of analysis and modeling research needed to achieve the goals of IMPROVE.

BACKGROUND. During the past three decades, the grid resolution of forecast models has increased with advances in computer technology, and model parameterizations of physical processes have become more sophisticated. Operational mesoscale models are now approaching the resolution necessary to resolve the dynamical processes and key terrain features that can have direct and significant impacts on precipitation. Several recent studies (Bruintjes et al. 1994; Colle and Mass 1996; Gaudet and Cotton 1998) have shown that, when run at sufficiently high resolution (down to ~10 km), mesoscale models can reproduce many of the observed features of precipitation structures over complex terrain. Yet, even when small-scale dynamical processes and complex terrain are adequately resolved, significant systematic deficiencies in model precipitation are often present (Colle et al. 1999; Colle and Mass 2000; Colle et al. 2000; Farley et al. 2000; Westrick and Mass 2001; Mass et al. 2002). For example, Colle et al. (2000) examined the model precipitation bias score, defined as simulated precipitation divided by observed precipitation at all available stations, for mesoscale model forecasts over the Pacific Northwest during the 1997–99 cool seasons (Fig. 1). This measure showed that skill increased as grid spacing was reduced from 36 to 12 km, but then skill decreased as grid spacing was further reduced to 4 km. Errors also seemed to depend on precipitation intensity.

These studies indicate that increased resolution alone is insufficient to produce accurate QPF fields. Another key aspect of mesoscale models that affects QPF is the parameterization of cloud and precipitation processes. Mesoscale models running at < 10 km resolution now treat most of the precipitation processes at the grid scale and, therefore, increasingly rely on BMP schemes, which until recently were used primarily in cloud resolving models. Remarkably, BMP schemes are now being used as subgrid-scale precipitation parameterizations in global climate models (Grabowski 2001; Khairoutdinov and Randall 2001). Thus, the success or failure of BMP impacts model simulations on all scales (cloud, mesoscale, and global).

In BMP schemes, the explicit prediction of a limited number of cloud and precipitation hydrometeor types is based on a complex array of empirically and theoretically derived sources, sinks, and exchange terms between those hydrometeor types. Early schemes predicted only the mixing ratios of the various hydrometeors (e.g., Cotton 1982; Lin et al. 1983; Rutledge and Hobbs 1983, 1984), whereas more recent schemes predict multiple moments of the size distributions, such as number concentration and mixing ratio (Ferrier 1994; Reisner et al. 1998; Meyers et al. 1997). In spite of their sophistication, evidence of flaws in BMP schemes arises often, particularly for higher-resolution simulations (e.g., Manning and Davis 1997; Colle and Mass 2000). A more complete list of known uncertainties and potential areas of improvement in BMP schemes is given in appendix A. Many flaws in BMP schemes have been revealed in case studies through indirect means, such as comparing forecast and observed precipitation, or satellite cloud cover with model-simulated cloud cover. Such comparisons can reveal problems in BMP schemes, but they do not identify the origin of those problems.

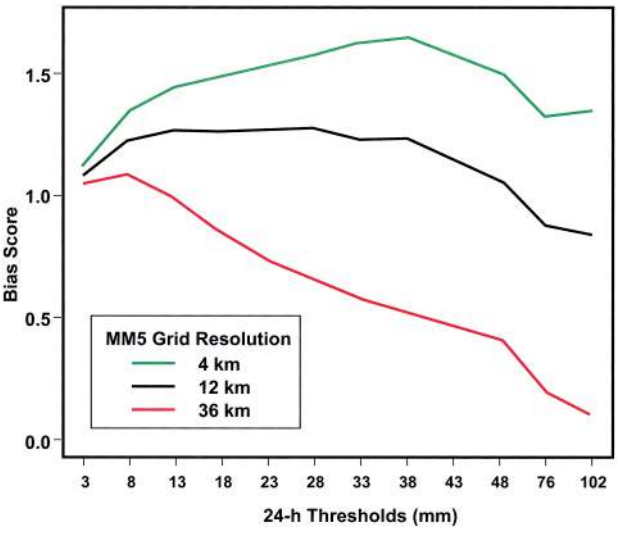

FIG. 1. The 24-h precipitation bias scores, as a function of 24-h precipitation threshold, for the 36-, 12-, and 4-km domains of the UW's Pacific Northwest MM5 model forecasts from 1 Jan 1998 through 15 Mar 1998 and 1 Oct 1998 through 8 Mar 1999. From Colle et al. (2000).

To determine the source of problems in a BMP scheme (and to correct them), it is necessary to compare microphysical processes and predicted hydrometeor distributions in model simulations with in situ and remotely sensed observations. In addition, it is critically important that the microphysical measurements be obtained concurrently with observations of wind, temperature, and humidity, so that errors in the simulated microphysics can be isolated from errors in other predicted fields.

Previous field programs that have included the study of cloud and precipitation microphysics [e.g., the CASCADE Project (Hobbs et al. 1971), CYCLES (Hobbs 1978), the Sierra Cooperative Pilot Project (Reynolds and Dennis 1986), the Coastal Observation and Simulation with Topography experiment (COAST; Bond et al. 1997), the Canadian Atlantic Storms Program (CASP-II, Cober et al. 1995), the Winter Icing and Storms Project (WISP; Rasmussen et al. 1992), and the Mesoscale Alpine Programme (MAP; Binder et al. 1996)] did not obtain sufficiently comprehensive data for the evaluation of mesoscale models, due to either a lack of key observing platforms and instruments or to different goals in the use of such platforms. The need for a focused field program has been recognized by both the Eighth and Ninth Prospectus Development Teams of the U.S. Weather Research Program, whose reports [Fritsch et al. (1998) and Droegemeier et al. (2000), respectively] have placed high priority on observational testing of the parameterizations of cloud and precipitation microphysics in numerical weather prediction models.

GOALS OF IMPROVE. To meet the need for comprehensive observational data for the testing and improvement of BMP schemes in mesoscale models, researchers at the University of Washington (UW) initiated IMPROVE, with the following goals:

1) To obtain comprehensive, quantitative measurements of cloud microphysical variables for a variety of precipitation events in which models provide a realistic simulation of the larger-scale structures. Such events should also produce a wide range of cloud and precipitation hydrometeor types and interactions.
2) To obtain corresponding dynamic and thermodynamic measurements (3D wind, temperature, and humidity fields) within and around the observed precipitation systems to provide the meteorological context in which the microphysical processes and precipitation events occurred.
3) To analyze the observational data to ascertain the physical processes leading to the development of precipitation, and the mixing ratios and size distributions of the various cloud and precipitation species.
4) To perform simulations of the observed cases with mesoscale models [the fifth-generation Pennsylvania State University–National Center for Atmospheric Research (Penn State–NCAR) Mesoscale Model (MM5) and eventually the Weather Research and Forecast Model (WRF)] that include a state-of-the-art BMP scheme [e.g., the Reisner et al. (1998) mixed-phase scheme], making use of the available observations in conjunction with advanced data assimilation techniques to maximize the accuracy of the simulations.
5) To compare the model forecasts of cloud and precipitation with the observations, both in terms of essential physical processes and quantitative amounts.
6) To make cost-effective and generally applicable improvements in BMP schemes in mesoscale models.

FIELD STUDY DESIGN. The need for comprehensive measurements was addressed through two IMPROVE field studies carried out in 2001. These field studies focused on clouds and precipitation forced by fronts and orography in the Pacific Northwest (see Fig. 2 for locations of study areas). In the winter, the Pacific Northwest is an ideal location to study precipitation systems both offshore and over orography, with numerous cyclonic storm systems making landfall from November through February.

IMPROVE-1, the Washington Offshore Frontal Field Study, was carried out off the coast of Washington State from 4 January to 14 February 2001. The advantage of studying frontal systems over an oceanic domain with weak sea surface temperature gradients is that they are driven by large-scale dynamical processes, which are typically well simulated in mesoscale models. Furthermore, because the lower boundary is spatially uniform, the structures of precipitation features can often be verified by observations even when modest timing and position errors are present in the model forecasts.

IMPROVE-2, the Oregon Cascades Orographic Field Study, was carried out in the Oregon Cascade Mountains from 26 November to 22 December 2001. Orographic precipitation systems are good candidates for IMPROVE studies because much of the forcing is tied to the terrain, which is precisely known. Thus, in situations where essentially steady flow impinges

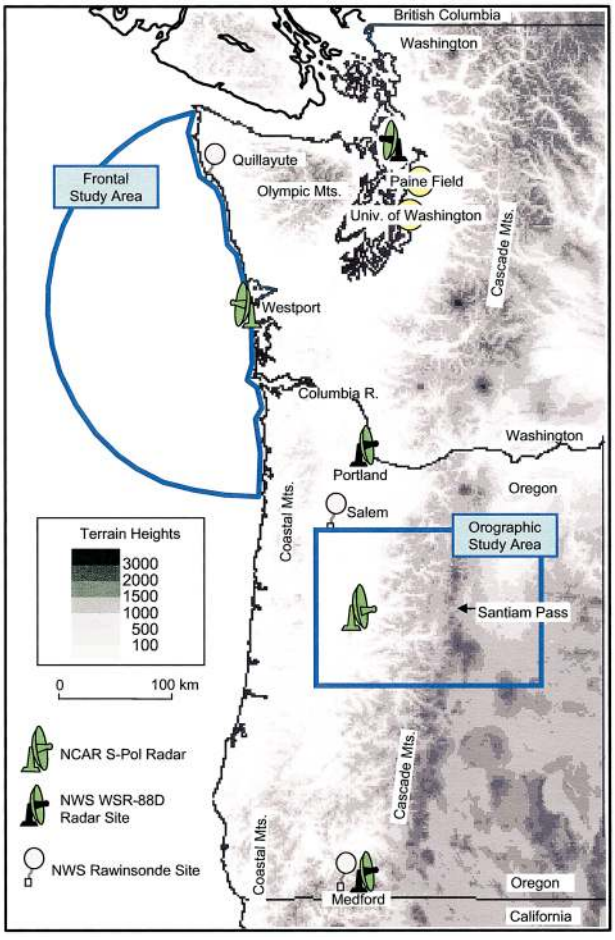

Fig. 2. Map of Pacific Northwest region, showing locations of the Frontal and Orographic Study Areas (heavy blue outlines), the UW, Paine Field, and NWS rawinsonde and WSR-88D radar sites.

on a topographic barrier and the upstream conditions are known, the dynamical response to that flow is highly deterministic, provided the forecast model can properly resolve the key terrain-forced dynamics (Colle and Mass 1996). In addition, terrain-forced flow produces large gradients in cloud microphysical variables and processes, which provides a good test bed for evaluating the model microphysics.

OBSERVATIONAL FACILITIES AND STRATEGIES. The IMPROVE field studies were designed to provide a multiscale suite of measurements to document the chains of events that lead to the formation of precipitation in a variety of weather situations. Because a prime goal of IMPROVE is to isolate model deficiencies associated with cloud microphysical processes from those associated with dynamics (e.g., terrain or synoptically forced vertical air motions), in situ and remotely sensed measurements of cloud and precipitation structures were required, together with simultaneous Doppler radar measurements of the kinematic fields. To satisfy these requirements, four key instrument platforms were deployed: the UW Convair-580 research aircraft, for in situ cloud microphysical measurements; the NCAR S-band dual-polarization Doppler radar (S-Pol), for remotely sensed measurements of clouds and precipitation; the NCAR Bistatic Radar Network (BINET), for ground-based Doppler velocity measurements (used only during IMPROVE-1); and the National Oceanic and Atmospheric Administration (NOAA) P-3 research aircraft, for airborne Doppler velocity measurements (used only during IMPROVE-2). These observing systems, as well as other supporting systems, are listed in Table 1, and are described in more detail below. The locations of all observing systems used during IMPROVE-1 and IMPROVE-2 are illustrated in Figs. 3 and 4, respectively.

The Convair-580 aircraft was well suited to obtain detailed in situ measurements of thermodynamic state parameters, cloud structure, and precipitation properties. Instruments of particular importance on the Convair-580 were the SPEC

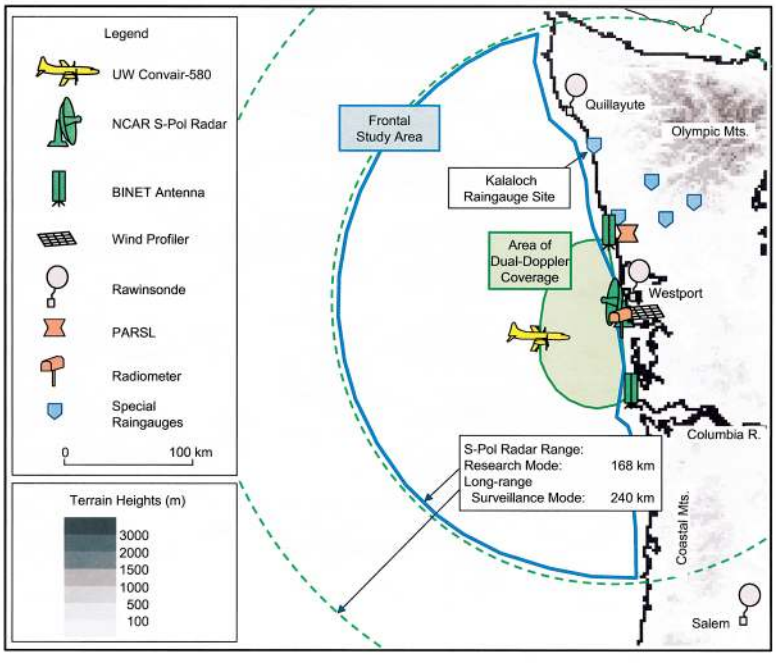

Fig. 3. Map of the IMPROVE-1 Frontal Study Area, showing locations of observational facilities.

Cloud Particle Imager (CPI), which provides detailed imagery of liquid and solid cloud and precipitation particles from 5 μm to 2.5 mm with a resolution of 2.3 μm (Lawson and Jensen 1998); the SPEC High Volume Precipitation Sampler (HVPS), which provides imagery and measurements of size spectrum and concentration for particles from 200 μm to 5 cm, with a resolution of 200 μm and a ~1 m^3 s^{-1} sampling rate at an aircraft speed of 100 m s^{-1} (Lawson et al. 1993); three Particle Measuring Systems (PMS) probes [the Forward Scattering Spectrometer Probe-100 (FSSP-100), 1D-C and 2D-C] for cloud particle imagery, concentration, and size spectrum measurements; and several instruments for measuring liquid water content of clouds. Figure 5 shows the size ranges of particles covered by these various instruments. Also aboard the Convair-580 were instruments for measuring aerosol properties, a 35-GHz (cloud) radar (during IMPROVE-1 only), and a cloud condensation nucleus (CCN) counter (installed and operated by NCAR personnel, during IMPROVE-2 only).

The NCAR S-Pol radar, which was located at Westport on the Washington coast (Fig. 3), has a wavelength of 10 cm and dual-polarization capabilities. The dual-polarized radar measurements can be used to infer information on particle type (wet snow, dry snow, irregular ice, rain) (Doviak and Zrnić 1993; Vivekanandan et al. 1999). In addition, a long-range, ground-based radar was essential for short-term weather forecasting, the guidance of research aircraft into precipitation

Table 1. Instrument platforms deployed during the two IMPROVE field studies.

Instrument platform	Source
UW Convair-580 research aircraft*,**	UW
NOAA P-3 research aircraft**	NOAA/AOC
NCAR S-Pol radar*,**	NCAR/ATD
NCAR BINET receivers*	NCAR/ATD
Ground-based snow crystal observations**	UW
NCAR integrated sounding systems (ISS)**	NCAR/ATD
ETL S-band profiler**	NOAA/ETL
ETL wind profilers*,**	NOAA/ETL
Special NWS rawinsondes*,**	NOAA/NWS
Special rawinsondes*,**	UW, U.S. Navy, PNNL, NCAR/RAP
NCAR scanning microwave radiometer*,**	NCAR/ATD
UW rain gauge network*,**	UW
UW disdrometer**	UW
PNNL remote sensing laboratory (PARSL)*,**	PNNL

AOC: Aircraft Operations Center. ATD: Atmospheric Technology Division. Laboratory; PNNL: Pacific Northwest National Laboratory.

* Operated during IMPROVE-1.

** Operated during IMPROVE-2.

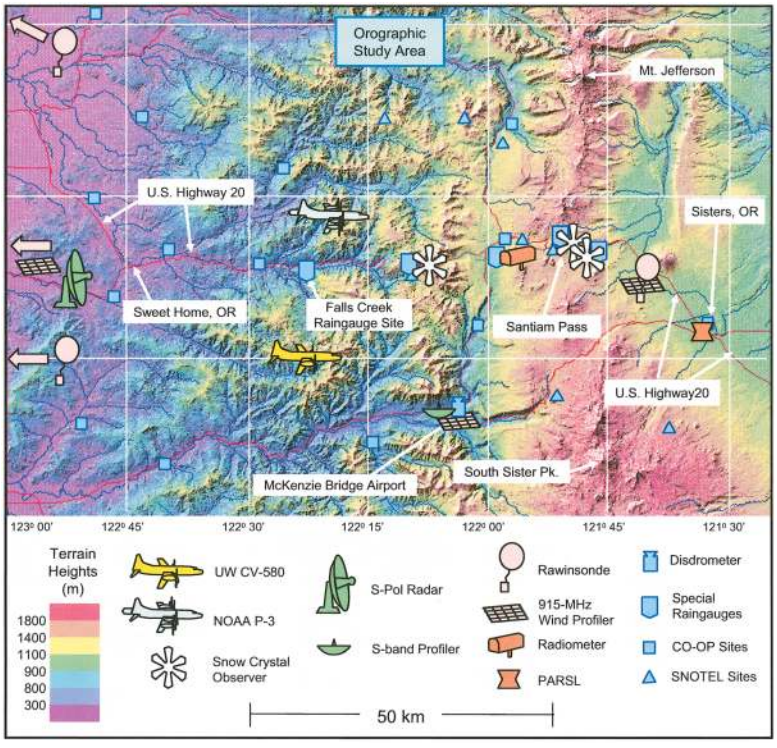

Fig. 4. Map of the IMPROVE-2 Orographic Study Area, showing locations of observational facilities.

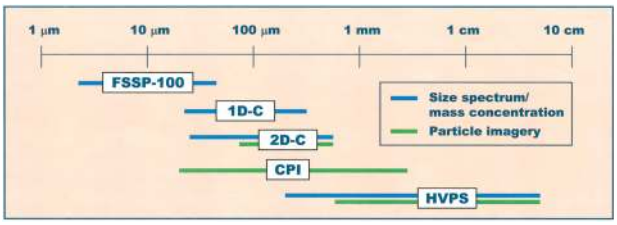

FIG. 5. Size ranges for cloud and precipitation measurements from instruments aboard the UW Convair-580 research aircraft.

systems, and the mapping of mesoscale precipitation structures and evolutions.

The 3D wind field measurements provided by Doppler radar are particularly important for IMPROVE, in that they are needed for comparison with model simulations to see if the model captures the essential kinematic context in which the precipitation developed. In IMPROVE-1, a ground-based system was employed that took advantage of the S-Pol radar's deployment on the Washington coast. Through the use of two bistatic receiving antennas in conjunction with a single ground-based Doppler radar, 3D air motions can be inferred using precipitation particles as targets (Wurman et al. 1993; Wurman 1994). For this purpose, bistatic receivers were located ~60 km north and south of the S-Pol radar. The bistatic antennas retrieved Doppler velocities from radar echoes with reflectivities $\geq$ 11 dBZ, within the area shaded in green in Figs. 3 and 6a. Due to the complex terrain in the IMPROVE-2 study area, an airborne dual-Doppler radar system was used instead of a ground-based system. The fore/aft-scanning Doppler X-band radar aboard the NOAA P-3 aircraft provided 3D air motions, particularly in those regions where the Convair-580 acquired cloud microphysical measurements. In addition, the P-3 was instrumented for basic-state parameter measurements, and had aboard PMS cloud and precipitation probes and an instrument for measuring cloud liquid water content, to augment the in situ microphysical measurements taken by the UW Convair-580.

In addition to the primary observing facilities described above, several supporting observational facilities were deployed during IMPROVE. These included the following:

- a number of special rain gauges;
- special 3-hourly rawinsonde launches from nearby National Weather Service (NWS) upper-air sites;
- special rawinsonde launches from a UW mobile rawinsonde unit, which operated near the S-Pol radar on the Washington coast during IMPROVE-1 and in the Willamette Valley, windward of the Cascade Mountain barrier, during IMPROVE-2;
- several 915-MHz wind profilers and radio acoustic sounding systems (RASSs) for continuous vertical profiles of wind and temperatures in the lower atmosphere [operated by both NOAA/Environmental Technology Laboratory (ETL) and NCAR];
- a radiometrics scanning microwave radiometer deployed by NCAR to measure column-integrated water vapor and cloud liquid water (Hogg et al. 1983; Heggli et al. 1983); and
- the Pacific Northwest National Laboratory's (PNNL) Atmospheric Remote Sensing Laboratory (PARSL), consisting of a 94-GHz vertically pointing cloud radar, a surface meteorology instrument suite, an optical rain gauge, a variety of radiometers

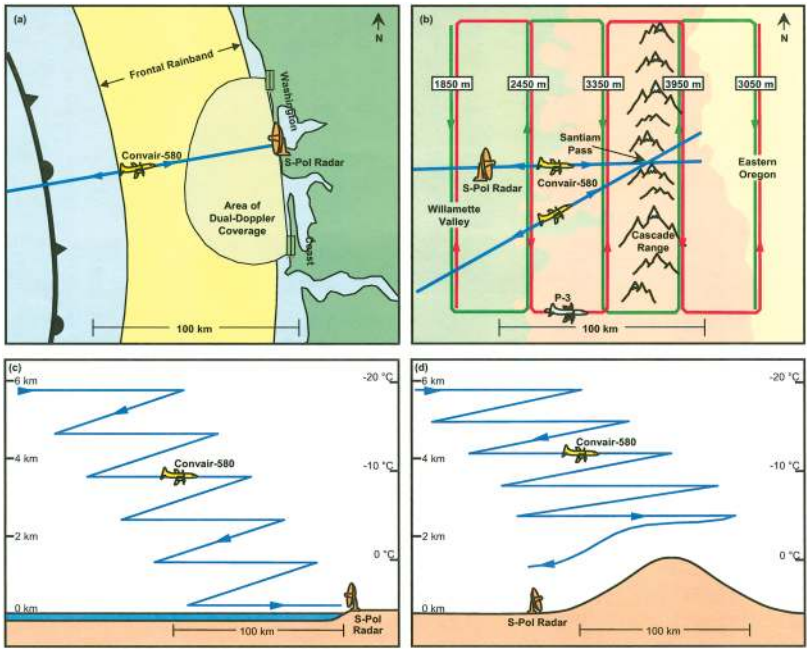

FIG. 6. Flight strategies employed during (left) IMPROVE-1 and (right) IMPROVE-2. Top panels show plan view and bottom panels show vertical cross sections. Dark blue lines are UW Convair-580 flight tracks; green and red lines are NOAA P-3 flight tracks. The temperatures indicated in the lower panels are typical for the indicated heights in the Pacific Northwest in winter.

for measurement of downwelling radiation, a total-sky imager, a microwave radiometer, and a ceilometer.

Additional facilities deployed only in IMPROVE-2 included the following:

- three mobile observers to identify snow crystal types reaching the surface at various locations across Santiam Pass;
- special NCAR integrated sounding system (ISS) sonde launches at Black Butte Ranch, Oregon, on the lee of the Cascades;
- a NOAA/ETL vertically pointing S-band Doppler radar (White et al. 2000), for providing information on precipitation structures aloft, located at McKenzie Bridge, Oregon; and
- a disdrometer for drop size distribution measurements at McKenzie Bridge.

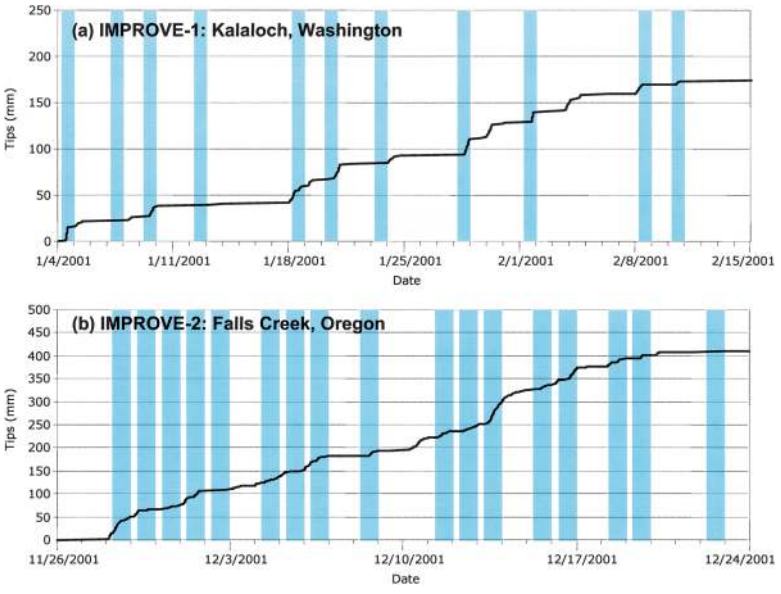

FIG. 7. Time series of precipitation accumulations at special rain gauge sites at (a) Kalaloch, WA, during IMPROVE-1, and (b) Falls Creek, OR, during IMPROVE-2. Blue bands show time periods of IMPROVE IOPs. Date hash marks are at 0001 LT. See Figs. 2 and 3 for locations.

The primary strategic challenges in IMPROVE were the flight-track design and targeting of the Convair-580 flight tracks for optimal microphysical data gathering; the flight-track design of the P-3 for optimal airborne dual-Doppler radar coverage (during IMPROVE-2); the optimal scan strategy for the S-Pol radar for weather surveillance, polarimetric studies, and (during IMPROVE-1) dual-Doppler coverage; and the timing of special sonde launches.

The Convair-580 flight tracks (Fig. 6) were designed to probe regions of precipitation along a stacked series of alternating horizontal and ascending flight legs oriented perpendicular to the band or terrain feature of interest and at a variety of vertical levels. When possible, the lowest leg was flown just below the melting level to ascertain the liquid precipitation rate. Nearly constant radio contact was maintained between flight scientists in the air and radar scientists on the ground. This communication, which was made possible by designing a flight strategy that kept the aircraft within a few hundred kilometers of the S-Pol radar site, was vital for guiding the aircraft into precipitation structures of interest.

In IMPROVE-1, the S-Pol radar performed sector volume scans in the offshore direction every half hour to produce BINET Doppler velocity data over the region shown in Fig. 3. In IMPROVE-2, the P-3 flew repeated "lawnmower" patterns of five north–south legs, each at a constant, minimum safe altitude (see Fig. 6b), to map out the Doppler velocity field on both sides of the Cascade Mountain barrier.

INTENSIVE OBSERVING PERIODS (IOPS). The winter of 2000/01 (during which IMPROVE-1 was conducted) was drier than normal in the Pacific Northwest. The following winter (during which IMPROVE-2 was conducted) was wetter than normal. However, both field phases provided a number of opportune weather systems for studying the targeted types of clouds and precipitation. Figure 7 shows precipitation time series from two selected special rain gauges, one from IMPROVE-1 and one from IMPROVE-2, with the time periods of the IOPs overlaid.

Precipitation during IMPROVE-1 was below normal due to a persistent split flow pattern. For example, Hoquiam, on the central Washington coast, received 16.7 and 10.8 cm during January and February, respectively, compared to climatological values of ~24.7 and 20.9 cm for these months. However, data from the IMPROVE rain gauge at Kalaloch on the Washington coast show that the IOPs generally coincided with periods of precipitation at the coast (Fig. 7). The correspondence was not perfect due in part to the persistent upper-level split flow, which caused some systems that were studied offshore to never make landfall or to weaken considerably upon landfall, whereas other systems made landfall after offshore observa-

tions were terminated. The majority of the IMPROVE-1 events were weak to moderately strong occlusions, which are climatologically the most frequent type of frontal passage in the area. Generally, model forecasting guidance was skillful and nearly all candidate weather systems were successfully targeted; a notable exception was a vigorous warm-frontal system on the evening of 3 February, which was missed due to poor model guidance.

The IMPROVE-2 period was considerably wetter than normal over central Oregon. Persistent zonal flow or troughing over the eastern Pacific brought a series of strong cyclones and fronts across the region during the first 3 weeks of the experiment. Stations in the Orographic Study Area generally received half a standard deviation above the normal precipitation amount for the month of December. For example, McKenzie Bridge, on the western slopes of the Oregon Cascades, received 37.9 cm during December, 10.8 cm above normal, while the nearby special IMPROVE-2 rain gauge at Falls Creek recorded a total of over 40.0 cm over the 4-week study period (Fig. 7b). Forecasting for IMPROVE-2 was challenging: some periods of heavy orographic precipitation were not well predicted by the models for forecast times over 24 h. However, the strongest and wettest weather systems were accurately targeted by IMPROVE operations.

A variety of flow regimes, frontal systems, and rainbands characterized both field phases of IMPROVE. The specific types of precipitation systems that were studied in all of the IOPs of both field phases are listed in appendix B. To illustrate the types of data gathered, two cases, one from each field phase of IMPROVE, are briefly described below. Detailed studies of these and other IMPROVE cases, and comparisons with numerical model outputs and algorithms, will be described in a future special issue of the *Journal of the Atmospheric Sciences*.

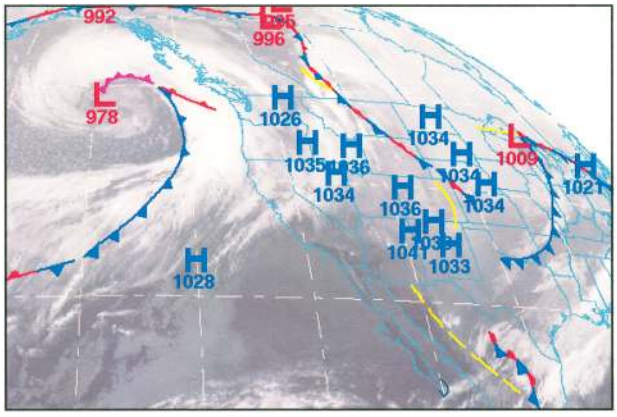

Fig. 8. Infrared satellite image and fronts analyzed by the National Centers for Environmental Prediction (NCEP) at 0000 UTC 2 Feb 2001.

IMPROVE-1: 1 February 2001. In midafternoon on 1 February, a strong occluded cyclone developed over the northeast Pacific Ocean, with an ill-defined warm front straddling the coast and a cold/occluded front moving steadily shoreward (Fig. 8). A deep cloud band is evident ahead of the front. A time–height cross section (Fig. 9), constructed from coastal soundings (at Quillayute and Westport, Washington; see Fig. 3), indicates that the frontal system was occluded as it came ashore, with a strong upper-level cold front forcing the main precipitation band, and a trailing surface occluded front making landfall several hours later. The warm-frontal surface can be seen as a stable layer (i.e., a layer of tightly packed contours of potential temperature and equivalent potential temperature) at ~800 hPa, ahead of the upper cold front. The rainband associated with the upper cold front was ~100 km wide, and was quite vigorous as it passed through the study area, with extensive, fairly uniform radar echoes of 35–40 dB*Z* over a wide area. The Convair-580 aircraft intercepted the rainband and flew a vertical stack of horizontal legs through it from 2347 UTC 1 February to 0253 UTC 2 February.

One issue that is of particular interest in IMPROVE is the role and importance of upper-level generating cells in the development of stratiform pre-

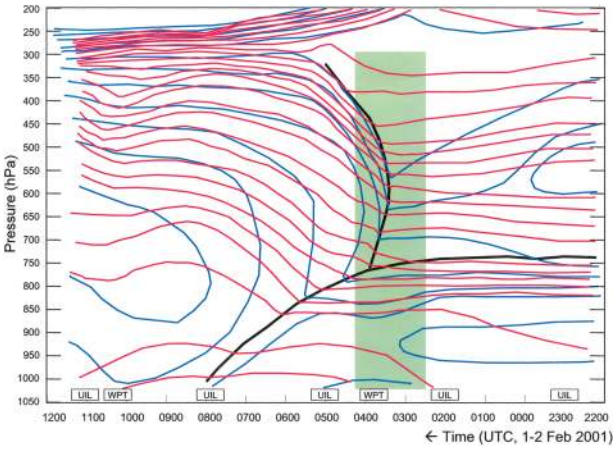

Fig. 9. Time–height cross section of onshore frontal passage on 1–2 Feb 2001, based on special IMPROVE soundings at Quillayute and Westport, WA. Red contours show potential temperature every 2 K; blue contours show equivalent potential temperature every 4 K. Solid black lines are frontal boundaries, and green shaded area shows the time period and vertical extent of precipitation associated with the upper cold-frontal rainband, as determined from S-Pol radar scans.

cipitation. Previous research has shown that contributions to precipitation mass by generating cells range from ~20% to 35% (Hobbs et al. 1980; Houze et al. 1981) depending on the strength of vertical air motions in the "feeder" zone. However, these cells tend to be small in scale and convective in nature, and it is not clear how well mesoscale models simulate stratiform precipitation that is influenced by generating cells aloft, and whether this phenomenon requires a separate parameterization scheme. While a detailed study of the process of ice particle formation within generating cells would require measurements not taken during IMPROVE (such as cloud and ice nuclei and small-scale vertical motions), the IMPROVE data can be used to examine the contribution of particles falling from generating cells to the growth of precipitation at lower levels. Analysis of the S-Pol radar data shows that the 1 February rainband was rife with generating cells at two altitudes. These can be seen most clearly in range–height indicator (RHI) scans from the S-Pol radar through the leading edge of the band (Fig. 10). A cirrus layer of generating cells is seen around 10-km altitude, and an altocumulus layer of generating cells at around 6-km altitude. Fallstreaks can be seen emanating from the generating cells, particularly from those in the altocumulus layer. In a later RHI scan (Fig. 10b), the fallstreaks are seen to penetrate the melting-layer bright band (at ~1–2 km) and appear to enhance the precipitation reaching the ground.

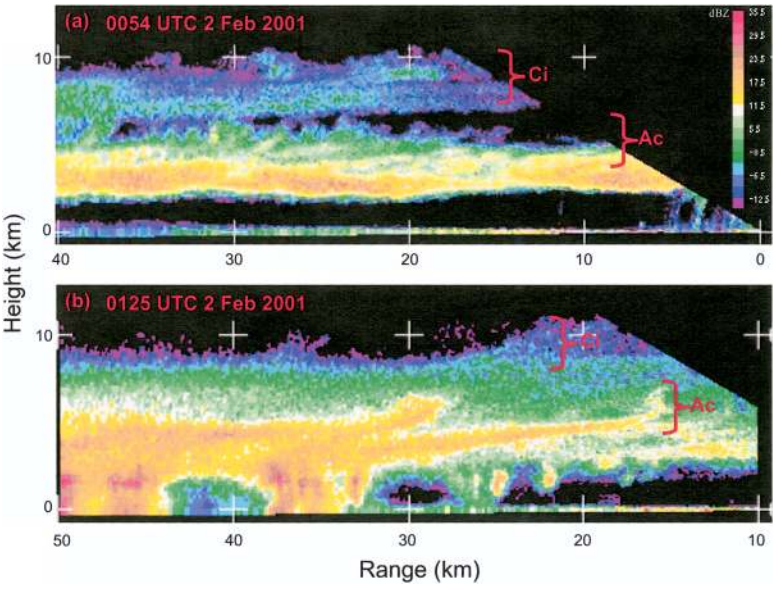

Fig. 10. RHI radar scans along the 240° azimuth at (a) 0054 and (b) 0125 UTC 2 Feb 2001, showing generating cells and fallstreaks in the easternmost (rightmost) part of the upper cold-frontal rainband. Two layers of generating cells are indicated: the cirrus layer of generating cells (labeled Ci), and the altocumulus layer of generating cells (labeled Ac).

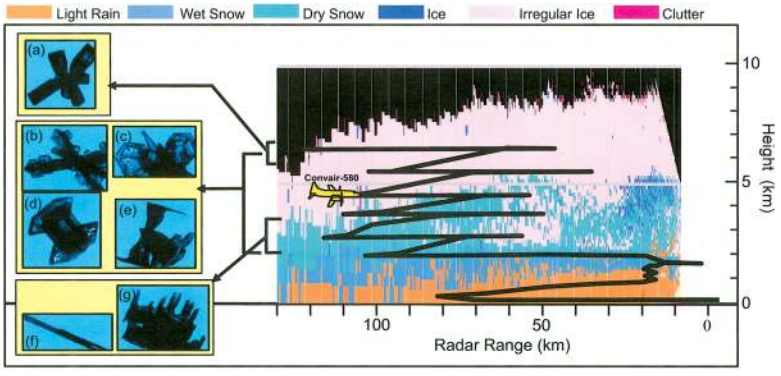

Fig. 11. Vertical cross section through the upper cold-frontal rainband of 1–2 Feb 2001. Color shades are the polarimetric particle identification result from an RHI scan of the NCAR S-Pol radar along the 250° azimuth of 0156 UTC 2 Feb 2001. Color code is shown at top. The magenta-colored clutter signal of the UW Convair-580 research aircraft can be seen immediately in front of the aircraft symbol. The black line shows the entire aircraft flight track in a reference frame moving with the rainband. Shown at left are several images of ice crystals that were recorded by the CPI on the aircraft in the altitude ranges indicated by the brackets.

Figure 11 shows a cross section through the rainband from the S-Pol radar along the same vertical section flown by the Convair-580. The color code shows the polarimetrically derived particle type identification (Vivekanandan et al. 1999). The precipitation regime is fairly uniform over a wide horizontal region, with the melting band (as seen in the transition from dry snow to wet snow to rain) occurring around 1.5 km. The system-relative aircraft flight track is also shown in Fig. 11, and the radar clutter signal from the aircraft can be seen as a narrow magenta-colored area at the nose of the overlaid aircraft symbol.

During the course of the 2 h and 20 min period that the Convair-580 flew in the rainband in temperatures

below freezing, over 90,000 images of ice crystals were generated by the CPI. Each image has been examined to determine crystal type and degree of riming. Figure 11 shows representative examples of some of the crystal types encountered during the flight. On the highest leg of the flight through the rainband, unrimed bullets (both radiating assemblages, as seen in Fig. 11a, and single bullets) were seen; these crystals likely originated in the cirrus-generating cells. Beneath that level, radiating assemblages of sideplanes (Fig. 11b) and assemblages of plates (Fig. 11c) were encountered, which probably originated in the altocumulus-generating cells. Lower still were columns and bullets with plates on their ends (Figs. 11d,e), which originated at higher levels. At the lowest levels, sheaths (Fig. 11f), as well as platelike crystals that originated aloft but subsequently grew sheaths and columns normal to their faces (Fig. 11g), were encountered. This type of information on crystal types, in conjunction with particle mass concentrations and size distributions, can be used to derive the growth history and spatial distribution of precipitation, which will be compared with model-simulated processes for the formation of the precipitation.

IMPROVE-2: 13 December 2001. On the afternoon of 13 December 2001 a vigorous frontal system, associated with a deep low pressure center that moved into Vancouver Island, came onshore in Oregon (Fig. 12). Although there did not appear to be a classical warm or occluded front with this system, the cold front had a tipped-forward structure in the lowest 3 km, not unlike the case discussed above from the IMPROVE-1 field study. The strongest synoptically forced precipitation occurred ahead of the upper cold front in a band that brought widespread stratiform precipitation to the study area for several hours. In addition to the synoptically forced precipitation, strong low-level flow with a large cross-barrier (westerly) component resulted in significant orographic enhancement of precipitation on the windward slopes of the Cascades. This situation is distinctly different from that typically seen in the Washington Cascades during the CASCADE Project (Hobbs et al. 1971), in which strong low-level cross-barrier flow and orographic precipitation development were typically not present until after frontal passage. In the 13 December 2001 case, the prefrontal regime had a combination of strong synoptically forced precipitation production aloft and strong orographic forcing below, resulting in heavy precipitation on the windward slopes of the Cascades. All of the IMPROVE-2 observational assets were deployed during this precipitation event. The Convair-580 aircraft performed two vertical stacks for in situ microphysical measurements, one in the prefrontal regime and one in the postfrontal regime, and the P-3 aircraft carried out nearly two complete lawnmower patterns for dual-Doppler measurements over the region surveyed by the Convair-580.

The combination of forcing mechanisms discussed above is evident in several aspects of the measurements. A time series from the microwave radiometer that was situated 7 km west of the Cascade crest (Fig. 13) illustrates the temporal evolution of column-integrated liquid water content. The time series indicates that the highest values of liquid water content (and, by inference, the strongest orographic forcing) occurred not in the postfrontal regime, but simultaneously with the rainband that was

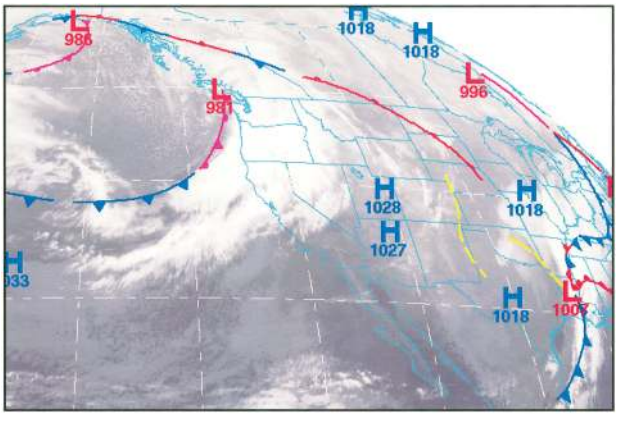

Fig. 12. Infrared satellite image, with NCEP-analyzed fronts overlaid, at 0000 UTC 14 Dec 2001.

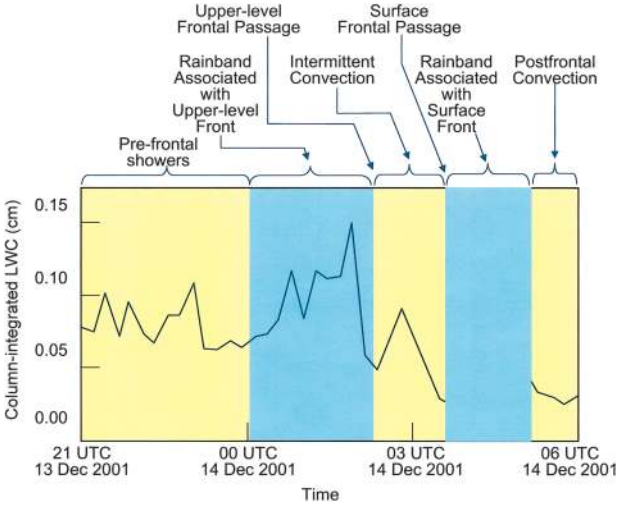

Fig. 13. Time series of vertically integrated liquid water content measured with a ground-based microwave radiometer (see Fig. 3 for location of radiometer) on 13–14 Dec 2001.

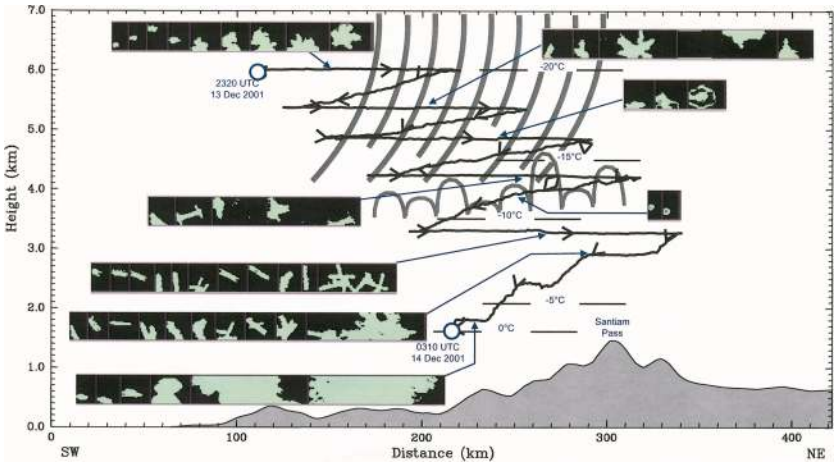

FIG. 14. Sample imagery from the PMS 2D-C probe aboard the UW Convair-580 aircraft on 13–14 Dec 2001. Solid line with arrow heads shows flight track. The sample particle images were observed at the points indicated by the blue arrows. The region of ice-phase precipitation is indicated by gray fallstreaks, and the top of the cloud liquid water region is indicated by the gray-scalloped cloud outline. Height is indicated on the left axis and temperature is indicated by the labeled horizontal line segments.

immediately ahead of the upper-level front. A cross section in the vertical plane in which the Convair-580 completed its first vertical stack is shown in Fig. 14. This flight was almost entirely within the rainband ahead of the upper-level front. Along the flight track several representative images from the PMS 2D-C probe are shown. The schematically drawn fallstreaks in Fig. 14 indicate the region where ice particles gen-

AIRCRAFT ICING DURING IMPROVE-2

Aircraft icing situations provided both an opportunity and a challenge in IMPROVE-2. Scientists from NCAR's Research Applications Program (RAP) participated in UW Convair-580 research flights during IMPROVE-2, in part to study the development of supercooled liquid water and in-flight icing conditions. Such conditions occurred on several flights during IMPROVE-2, particularly during postfrontal orographic precipitation events. However, the encountering of supercooled liquid water was a mixed blessing for IMPROVE. While it provided an opportunity to study this important microphysical regime, it also presented a major operational challenge. Often, severe aircraft icing was experienced by both the Convair-580 and NOAA P-3 research aircraft as they flew in supercooled clouds. As illustrated by the ice cap removed from the nose of the P-3 after a research flight (see cover photo of this issue), considerable ice sometimes accumulated on aircraft windshields (Fig. SB1), propellers, and wings. Icing resulted in the failure of several aircraft components, including a deicing boot on a P-3 prop and an airspeed indicator on the Convair-580. On occasion, heavy icing also affected some of the meteorological sensors. However, most of the sensors were fitted with heaters to mitigate icing-related problems.

While icing conditions were to be expected in IMPROVE-2, they were nonetheless disquieting to aircraft flight and science crew. Ice breaking off and impacting on the fuselage of the aircraft often produced loud bangs, and on occasion icing had a noticeably detrimental impact on the flight characteristics of the aircraft. Certainly not far from the minds of the aircraft crew were thoughts of a fatal crash of a cloud research aircraft that occurred on the windward slopes of the Sierra Nevada in 1980 (Telford 1988), in icing conditions not unlike those encountered in IMPROVE-2. However, the experienced crew of both aircraft rightly prioritized safety above science, and did not hesitate to pull out of flight legs during which excessive ice accumulation occurred, to descend to warmer regions and melt off accumulated ice.

FIG. SB1. Ice accumulates on the windshield of the NOAA P-3 aircraft during the 18 Dec 2001 IMPROVE-2 research flight.

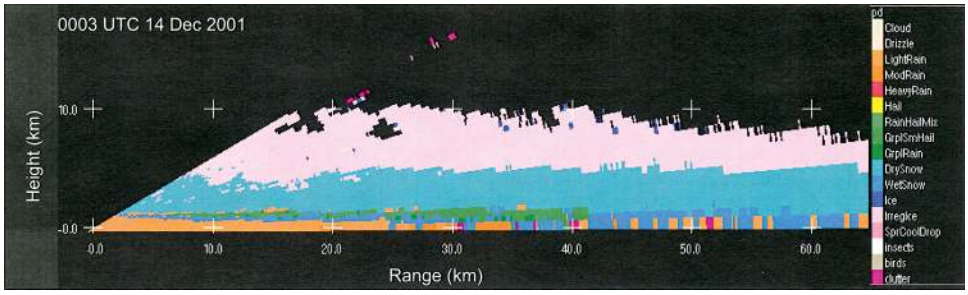

Fig. 15. Polarimetric particle identification result from an RHI scan of the NCAR S-Pol radar along the 85° azimuth at 0003 UTC 14 Dec 2001. Color code for particle type is shown at right.

erated by the rainband either fell into the flight region from above or developed within the flight region. The schematically drawn cloud boundary indicates the top of a region where the aircraft encountered significant supercooled liquid water. Examples of liquid water droplet images are seen just below the 4-km level. Beneath that level, both high supercooled liquid-water and high ice-particle concentrations (e.g., needles and aggregates thereof at around 3 km) coexisted, indicating the vigor of the liquid-water-replenishing orographic uplift. Some evidence of rimed aggregates (i.e., aggregates with few interstitial spaces) is seen just above the freezing level. Also, a polarimetrically derived particle identification plot from an RHI scan of the S-Pol radar in the upslope direction (Fig. 15) indicated the existence of graupel (green and dark green colors) just above the melting band.

A high-resolution time series of reflectivity (Fig. 16a) from the S-band vertical profiler at McKenzie Bridge (approximately 20 km west of the Cascade crest) indicates a deep continuous layer of echo with a bright band at a height of 1.7 km prior to 0200 UTC 2 February. The radial velocity data

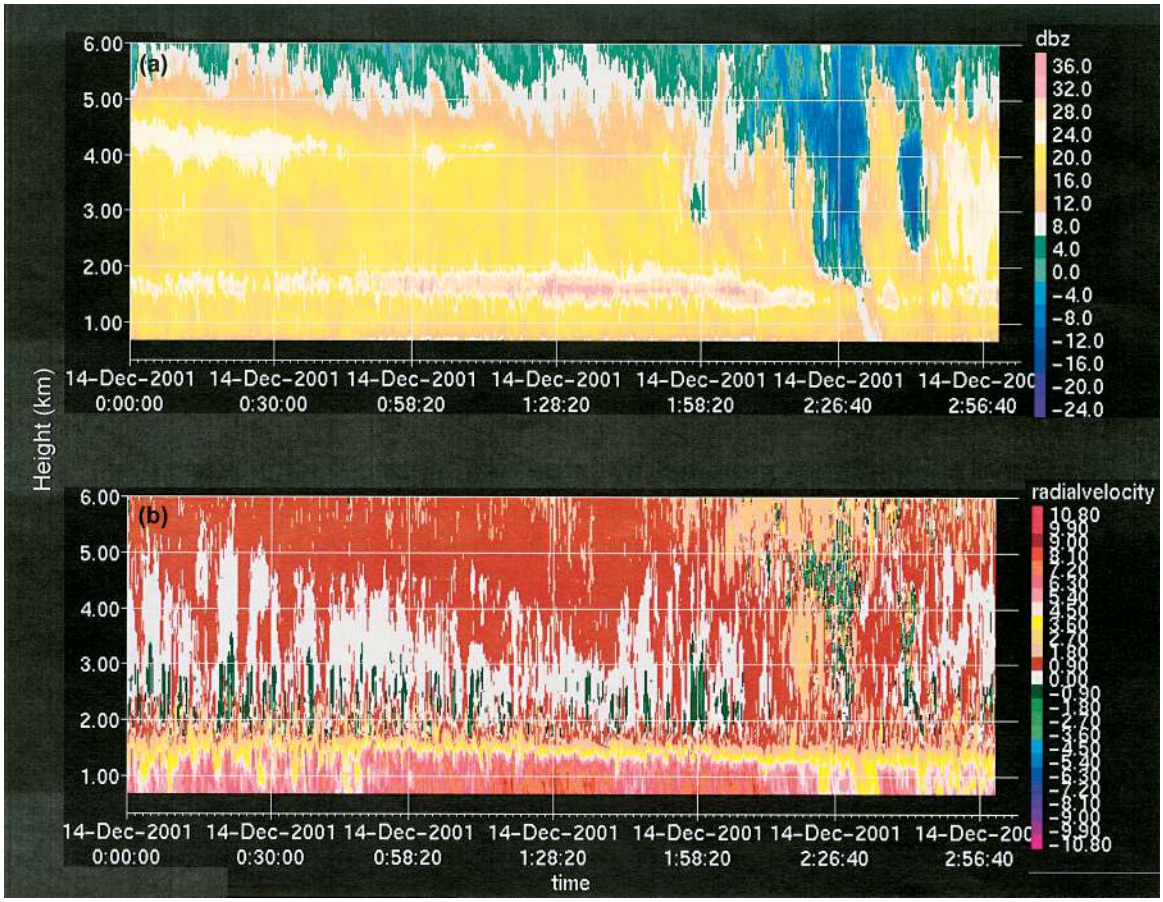

Fig. 16. Time–height cross sections of measurements from the S-band profiler (see Fig. 3 for location) on 14 Dec 2001: (a) reflectivity; (b) Doppler vertical velocity. Height is above sea level, times are in UTC, and positive velocity values are downward.

(Fig. 16b) showed a considerable depth between 2.0 and 3.5 km in which the radial velocity was zero or upward, indicating updrafts of a meter per second or more. The image shows a pattern of closely spaced, convective-scale cells of upward air velocity, just above the melting layer. This pattern is consistent with the appearance of graupel at this level in the S-Pol particle identification field, which provides another indication of both the large input of ice particles from aloft and the strong production of supercooled liquid water by orographic uplift.

SOME PRELIMINARY MODELING STUDIES. Nested-grid model simulations of both the 1 February 2001 and 13 December 2001 cases described above have been run with horizontal grid spacings of 36, 12, and 4 km, and vertical grid spacing

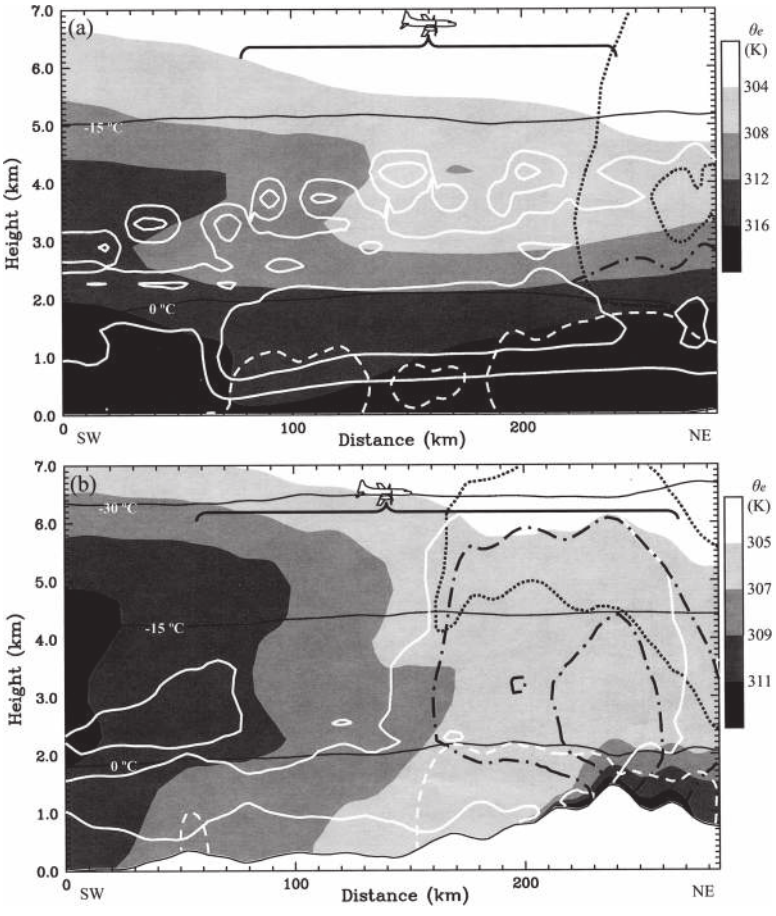

FIG. 17 (TOP). Cross sections through precipitation events simulated by the MM5 model on (a) 1–2 Feb 2001 and (b) 13–14 Dec 2001. Shading indicates equivalent potential temperature (θ_e), with key given at right. Thin black lines are temperature in °C. Hydrometeor mixing ratios are indicated by contour types as follows: cloud water, solid white; rain, dashed white; snow, short-dashed black; and graupel, dash–dot black. Contour values in (a) are 0.1 g kg^{-1} for all types, with a second contour of 0.3 g kg^{-1} for cloud water and snow. Contour values in (b) are 0.2 g kg^{-1} for all types, with a second contour of 1.0 g kg^{-1} for cloud water and graupel. Regions covered by the UW Convair-580 flights are indicated by an aircraft symbol and large brace.

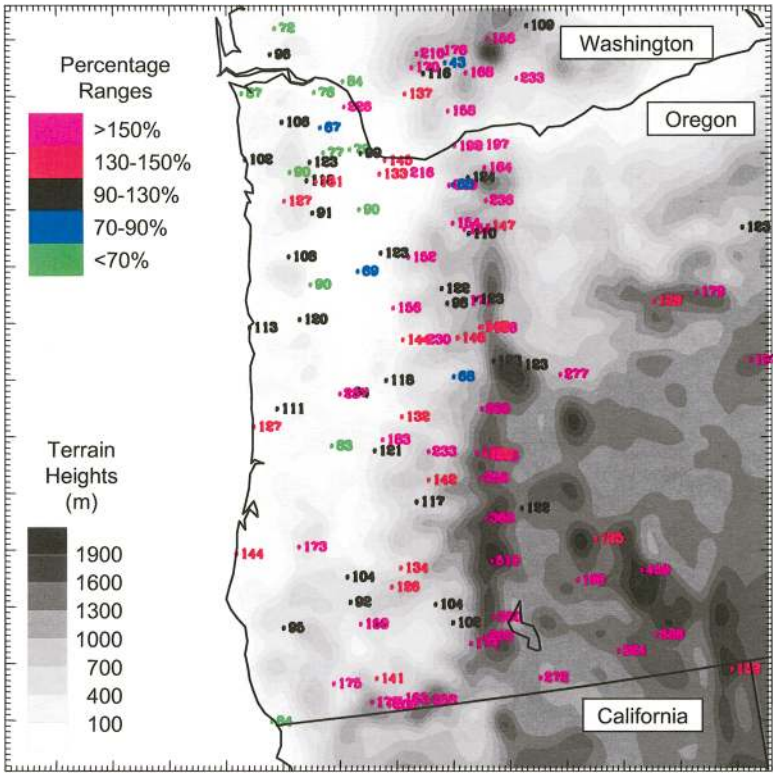

FIG. 18 (BOTTOM). Precipitation accumulated during the period 1400 UTC 13 Dec 2002–0800 UTC 14 Dec 2002 from a 4-km MM5 model simulation, expressed as a percentage of observed precipitation at rain gauge sites in the vicinity of the IMPROVE-2 study area. Terrain heights are shown at lower left, and color coding of percentage ranges is shown at upper left.

COOPERATIVE EFFORTS

In addition to the primary goals of IMPROVE, several participants were able to incorporate other research and operational efforts into the field studies, which took advantage of the substantial observational assets provided by IMPROVE.

- **During IMPROVE-1, the NWS was keenly interested in operational use of the S-Pol radar that was deployed on the Washington coast, because it was placed in a location that fills in a major gap in coverage of the operational Weather Surveillance Radar-1988 Doppler (WSR-88D) network, and it has polarimetric capabilities. NCAR set up a Zebra display workstation in the NWS Seattle office, providing NWS with real-time access to S-Pol reflectivity, Doppler velocity, particle identification, and rainfall estimation plots. These products were examined routinely by forecasters and were helpful in predicting some heavy precipitation events on the Olympic Peninsula. The NWS in turn contributed to IMPROVE with forecasting assistance and with special sonde launches at Quillayute, WA, and Salem, OR, during both field phases of IMPROVE.**
- **The PNNL deployed their PARSL remote sensing observing system to test its suite of cloud-sensing measurements against in situ microphysical measurements from the aircraft. They also contributed surface and radar observations to the IMPROVE dataset, and provided a sounding receiver unit during IMPROVE-2.**
- **In conjunction with the Pacific Landfalling Jets Experiment (PACJET), which occurred along the west coast of the United States simultaneously with IMPROVE-1, NOAA/ETL deployed a 915-MHz wind profiler site at Westport, approximately 1 km from the S-Pol radar site. This site benefited both PACJET and IMPROVE, and provided an opportunity to perform intercomparison between the wind profiles provided by a 915-MHz wind profiler and by velocity–azimuth display (VAD) scans from a 10-cm radar (such as S-Pol or WSR-88Ds).**
- **During IMPROVE-2, NCAR's Research Applications Program (RAP) installed a CCN counter on the Convair-580 and, on some missions, CCN concentrations were measured in the westerly flow upstream of the Cascade Range prior to cloud formation, and in cloud-processed air in the lee of the Cascades. RAP also studied aircraft icing conditions during IMPROVE-2 (see sidebar on aircraft icing).**
- **Sandra Yuter (UW) deployed two disdrometers at McKenzie Bridge, collocated with the NOAA/ETL profilers and surface meteorology instruments, to add another precipitation site to her dataset on raindrop size distributions in diverse locations.**

≤ 36 hPa. Preliminary work has been completed to verify that the simulations captured the essential kinematic, thermal, and moisture structures that were observed. Vertical cross sections of the two model simulations are shown in Fig. 17. The model cross sections are in the same vertical plane as the Convair-580 flight tracks along which cloud microphysical data were collected. In both model simulations, the equivalent potential temperature (θ_e) pattern shows an occluded baroclinic structure entering the picture from west to east (left to right), with an axis of maximum θ_e sloping eastward with height in the lowest 4 km. Although the two cases share this basic synoptic structure, they differ in terms of the presence of orographic forcing in the IMPROVE-2 case, and in terms of greater static stability in the IMPROVE-1 case (note that in Fig. 17a the θ_e contours are more closely spaced in the vertical and the temperature contours more widely spaced, both of which indicate greater stability). Both model simulations produce regions of cloud water, rain, cloud ice, snow, and graupel, with significant amounts of supercooled liquid water.

Precipitation amounts predicted by the MM5 model at 4-km grid spacing for 13–14 December 2001 were checked using over 100 hourly cooperative observer (COOP) and snow telemetry (SNOTEL) sites across Oregon and southern Washington (Fig. 18). The MM5 precipitation accumulated between 1400 UTC 13 December and 0800 UTC 14 December was interpolated to the observation sites as in Colle et al. (1999). Figure 18 shows the percentage of the observed precipitation produced by the model at the observation sites. The model overpredicted the precipitation over the Cascades, while there is some underprediction in the lee of the coastal range. The overprediction occurred even though the model-simulated crest-level flow was 5–10 m s^{-1} weaker than observed (not shown), which suggests deficiencies in the model microphysics.

CURRENT AND FUTURE RESEARCH DIRECTIONS. IMPROVE research is now focusing on two main efforts: analysis of the observational data and model simulations. Both the observational and modeling studies can be divided into three main objectives: 1) to understand and quantify the mesoscale processes that lead to the development and modulation of precipitation, 2) to understand and quantify the microphysical processes that lead to the develop-

ment of precipitation, and 3) to quantify the spatial and temporal distributions of cloud and precipitation hydrometeors and precipitation fallout at the surface. For each of these objectives, the goal is the comparison of model outputs with the observations. The mesoscale kinematic, thermal, and moisture evolution in the model simulation will be checked and errors reduced to a minimum; any remaining errors in the precipitation evolution can be attributed to the BMP scheme used in the model simulation. For example, specific phenomena that will be examined are the model's handling of mountain waves in the orographic cases (Reinking et al. 2000) and of upper-level instability and generating cells in deep frontally forced precipitation systems (Hobbs et al. 1980; Houze et al. 1981). Incorrect kinematic fields associated with these phenomena will likely affect the accuracy of the model-simulated precipitation, irrespective of possible problems in the BMP scheme. We will attempt to correct these kinematic and dynamical deficiencies using tools such as 4D data assimilation on the outer grids. Adequate simulation of mountain waves may also require the use of a higher-resolution model grid (~1 km). The microphysical processes and quantitative outputs from the model will be compared with observations to determine where the BMP scheme is handling precipitation development properly and where it is not. These comparisons should reveal any weaknesses in the BMP schemes and motivate improvements. The revised schemes will then be tested on other IMPROVE cases and in an operational forecasting environment.

SUMMARY. During the past several years, there has been increasing evidence of deficiencies in bulk microphysical parameterizations in numerical weather prediction models. Improvements in these parameterizations have been difficult because coincident and comprehensive measurements of both the basic-state flow and microphysical parameters have not been available. In response to the need for such data, two field campaigns were carried out: an offshore frontal precipitation study off the Washington coast in January–February 2001, and an orographic precipitation study in the Oregon Cascade Mountains in November–December 2001. Twenty-eight IOPs yielded uniquely comprehensive data that include in situ airborne observations of cloud and precipitation microphysical parameters; remotely sensed reflectivity, dual-Doppler, and polarimetric quantities from both the surface and aloft; upper-air wind, temperature, and humidity data from balloon soundings and vertical profilers; and a wide variety of surface-based meteorological, precipitation, and microphysical data. These data are being used to test mesoscale model simulations of the observed storm systems and, in particular, to evaluate and improve bulk microphysical parameterization schemes used in the models. These studies should lead to improved quantitative precipitation forecasting in research and operational forecast models.

A comprehensive description of IMPROVE and its datasets are available on the IMPROVE Web site (http://improve.atmos.washington.edu).

ACKNOWLEDGMENTS. Thanks are due to NCAR (Atmospheric Technology Division and Research Applications Program), NOAA/ETL, and PNNL for providing and staffing experimental facilities; the NWS and the Naval Pacific Meteorology and Oceanography Facility at Whidbey Island, for launching special rawinsondes on request; the NOAA P-3 team; the Convair-580 pilots; and the Federal Aviation Administration/Seattle Air Route Traffic Control Center for cooperation in the use of airspace. We also thank staff members and graduate and undergraduate students from the UW for assistance with field studies and data analysis.

IMPROVE is funded by the Mesoscale Dynamic Meteorology Program (Stephan Nelson, program director) and the Physical Meteorology Program (Roddy R. Rogers, program director) of the Division of Atmospheric Sciences, of the National Science Foundation, and by the U.S. Weather Research Program. NCAR's participation in IMPROVE was sponsored by the National Science Foundation and the Federal Aviation Administration.

APPENDIX A: SOME IMPORTANT MICROPHYSICAL ISSUES.

A number of outstanding issues regarding cloud microphysical processes have arisen out of observational and modeling/parameterization studies. These issues provided specific areas for consideration by the IMPROVE project. Some of the more important areas and related questions are listed below.

Autoconversion of cloud water to rainwater.

- How important is it to predict or specify variable CCN concentrations (Chen and Lamb 1994; Rasmussen et al. 2002)?
- How important is it to account for the effects of giant CCN and CCN activation characteristics (e.g., Cotton et al. 2003), instead of the common assumption that cloud droplet concentration equals CCN concentration?
- What is the general impact of increasing sophistication in the representation of autoconversion in

model simulations, from the simplest scheme (Kessler 1969) to increasingly complex schemes (e.g., Manton and Cotton 1977; Khairoutdinov and Kogan 2000)?
- Can/should aging effects be incorporated into the autoconversion process (Straka and Rasmussen 1997)?
- Do entrainment effects (Baker and Latham 1979; Telford and Wagner 1981) significantly hasten cloud-to-rain conversion?

Ice initiation.
- Several approaches to relating ice nucleus concentrations to temperature and/or humidity have been proposed (Fletcher 1962; Cooper 1986; Meyers et al. 1992). Which, if any, produces results that are most consistent with observations of ice particles in clouds?
- Can/should aging effects be incorporated into the ice initiation process (e.g., Hobbs and Rangno 1985)?
- How important is the prediction of number concentration of ice particles (as opposed to predicting just mass concentration)?
- Rutledge and Hobbs (1983) artificially inserted the effects of generating cells into an idealized numerical simulation of the seeder–feeder process. To what extent do current models handle the effect of generating cells aloft on stratiform precipitation, and does the process require a separate parameterization?
- Should ice nucleus number concentrations be treated as a predictive variable to more appropriately account for the depletion of ice nuclei (Rasmussen et al. 2002)?

Ice enhancement.
- Ice splinter reproduction due to riming (Hallett and Mossop 1974; Mossop 1985) is the only ice enhancements process (if any) that is currently included in BMP schemes. However, there is evidence that ice enhancement can occur much faster than the Hallett–Mossop laboratory studies suggest (Hobbs and Rangno 1985, 1990; Rangno and Hobbs 1991, 1994). How should ice enhancement be parameterized in numerical models?

Ice particle terminal velocities.
- Both empirical (e.g., Locatelli and Hobbs 1974; Zikmunda and Vali 1972) and theoretical (e.g., Mitchell 1996; Khvorostyanov and Curry 2002) expressions exist for relating ice particle size and terminal velocity for various crystal habits, degree of riming, and degree of aggregation. The challenge in designing BMP schemes is to assign a single terminal velocity relationship to each bulk hydrometeor category.

Assumed particle size distributions.
- Various levels of sophistication have been used in BMP schemes:
  1) exponential, with constant slope parameter;
  2) exponential, with slope parameter diagnosed from mixing ratio;
  3) exponential, with number concentration predicted; and
  4) gamma distribution with number concentration predicted and width parameter specified.

Which approach is most appropriate and/or necessary for each hydrometeor type?

- Should microphysical schemes move beyond the traditional "bulk" approach? Other innovative approaches have also been used, such as Feingold et al.'s (1998) use of a set of basis functions to define the size distributions and allow them to evolve with time.

Aggregation.
- Aggregation can have a significant effect on snow particle density [and thus, terminal fall velocity, as discussed by Rasmussen et al. (1999)] and snowflake size distribution (e.g., Lawson et al. 1998). Aggregation is also temperature dependent (Hobbs et al. 1974). How is aggregation best represented in BMP schemes?

By utilizing the extensive and unique data gathered during the IMPROVE field studies, we will address these and other questions in an effort to improve BMP schemes in mesoscale forecast models.

APPENDIX B: SUMMARY OF INTENSIVE OBSERVATION PERIODS (IOPS). A variety of flow regimes, frontal systems, and rainbands characterized both field phases of IMPROVE. The specific types of precipitation systems that were studied in all of the IOPs of both field phases are listed in Tables B1 and B2.

REFERENCES

Baker, M. B., and J. Latham, 1979: The evolution of droplet spectra and the rate of production of embryonic raindrops in small cumulus clouds. *J. Atmos. Sci.,* **36,** 1612–1614.

TABLE B1. IOPs carried out during IMPROVE-1.

IOP no.	Date (2001)	Types of frontal rainbands studied
1	4 Jan	Warm-sector rainbands and cold-frontal rainband
2	7 Jan	Upper cold-frontal rainband
3	9 Jan	Upper cold-frontal and occluded-frontal rainbands
4	12 Jan	Upper cold-frontal rainband
5	18 Jan	Warm-frontal and occluded-frontal rainbands
6	20 Jan	Occluded-frontal rainband and warm-frontal rainband
7	23 Jan	Rainbands associated with a cutoff low
8	28 Jan	Two prefrontal rainbands and a narrow cold-frontal rainband
9	1 Feb	Upper cold-frontal rainband
10	8 Feb	Warm-frontal and cold-frontal rainbands
11	10 Feb	Narrow and wide cold-frontal rainbands

TABLE B2. IOPs carried out during IMPROVE-2.

IOP no.	Date (2001)	Types of orographic precipitation studied
1	28 Nov	Occluded-frontal band over mountains
2	29 Nov	Postfrontal cross-barrier flow forcing shallow orographic precipitation
3	30 Nov	Warm-advection cross-barrier flow with two embedded rainbands
4	1 Dec	Postfrontal cross-barrier flow forcing deep orographic precipitation
5	2 Dec	Passage of comma cloud over orographic barrier
6	4 Dec	Postfrontal cross-barrier flow forcing deepening orographic precipitation
7	5 Dec	Passage of upper cold-frontal and occluded-frontal bands over mountains
8	6 Dec	Postfrontal cross-barrier flow forcing deep orographic precipitation
9	8 Dec	Passage of two cold-frontal rainbands over mountains
10	11 Dec	Postfrontal cross-barrier flow forcing shallow orographic precipitation
11	12 Dec	Warm-advection cross-barrier flow with two embedded rainbands
12	13 Dec	Passage of upper cold-frontal and occluded-frontal bands over mountains
13	15 Dec	Warm-advection cross-barrier flow forcing cellular orographic precipitation
14	16 Dec	Warm-advection prefrontal precipitation, then narrow cold-frontal band
15	18 Dec	Passage of prefrontal band and postfrontal comma cloud over mountains
16	19 Dec	Passage of warm-frontal band (perpendicular to ridge) over mountains
17	22 Dec	Narrow cold-frontal band dissipating as it passed over mountains

Binder, P., and Coauthors, 1996: MAP—Mesoscale Alpine Programme design proposal. MAP Programme Office, 77 pp. [Available from MAP Programme Office c/o Swiss Meteorological Institute, Krähbühlstrasse 58, CH-8044 Zürich, Switzerland.]

Bond, N. A., and Coauthors, 1997: The Coastal Observation and Simulation with Topography (COAST) experiment. *Bull. Amer. Meteor. Soc.,* **78,** 1941–1955.

Bruintjes, R. T., T. L. Clark, and W. D. Hall, 1994: Interactions between topographic airflow and cloud/precipitation development during the passage of a winter storm in Arizona. *J. Atmos. Sci.,* **51,** 48–67.

Chen, J.-P., and D. Lamb, 1994: Simulation of cloud microphysical and chemical processes using a mul-

ticomponent framework. Part I: Description of the microphysical model. *J. Atmos. Sci.,* **51,** 2613–2630.
Cober, S. G., G. A. Isaac, and J. W. Strapp, 1995: Aircraft icing measurements in East Coast winter storms. *J. Appl. Meteor.,* **34,** 88–100.
Colle, B. A., and C. F. Mass, 1996: An observational and modeling study of the interaction of low-level southwesterly flow with the Olympic Mountains during COAST IOP 4. *Mon. Wea. Rev.,* **124,** 2152–2175.
——, and ——, 2000: The 5–9 February 1996 flooding event over the Pacific Northwest: Sensitivity studies and evaluation of the MM5 precipitation forecasts. *Mon. Wea. Rev.,* **128,** 593–617.
——, K. Westrick, and C. F. Mass, 1999: Evaluation of MM5 and Eta-10 precipitation forecasts over the Pacific Northwest during the cool season. *Wea. Forecasting,* **14,** 137–154.
——, C. F. Mass, and K. J. Westrick, 2000: MM5 precipitation verification over the Pacific Northwest during the 1997–99 cool seasons. *Wea. Forecasting,* **15,** 730–744.
Cooper, W. A., 1986: Ice initiation in natural clouds. *Precipitation Enhancement—A Scientific Challenge, Meteor. Monogr.,* No. 43, Amer. Meteor. Soc., 29–32.
Cotton, W. R., 1982: Colorado State University three-dimensional cloud/mesoscale model. Part 2: Ice phase parameterization. *J. Rech. Atmos.,* **16,** 295–320.
——, and Coauthors, 2003: RAMS 2001: Current status and future directions. *Meteor. Atmos. Phys.,* **82,** 5–29.
Cressman, G., 1959: An operational objective analysis system. *Mon. Wea. Rev.,* **87,** 367–374.
Doviak, R. J., and D. S. Zrnić, 1993: *Doppler Radar and Weather Observations.* 2d ed. Academic Press, 562 pp.
Drogemeier, K. K., and Coauthors, 2000: Hydrological aspects of weather prediction and flood warnings: Report of the Ninth Prospectus Development Team of the U.S. Weather Research Program. *Bull. Amer. Meteor. Soc.,* **81,** 2665–2680.
Farley, R. D., D. L. Hjermstad, and H. D. Orville, 2000: Numerical simulation of a 4-day early spring storm period in the Black Hills. *J. Appl. Meteor.,* **39,** 1299–1317.
Feingold, G., R. L. Walko, B. Stevens, and W. R. Cotton, 1998: Simulations of marine stratocumulus using a new microphysical parameterization scheme. *Atmos. Res.,* **47–48,** 505–528.
Ferrier, B. S., 1994: A double-moment multiple-phase four-class bulk ice scheme. Part I: Description. *J. Atmos. Sci.,* **51,** 249–280.
Fletcher, N. H., 1962: *Physics of Rain Clouds.* Cambridge University Press, 386 pp.
Fritsch, J. M., and Coauthors, 1998: Quantitative precipitation forecasting: Report of the Eighth Prospectus Development Team, U.S. Weather Research Program. *Bull. Amer. Meteor. Soc.,* **79,** 285–299.
Gaudet, B., and W. R. Cotton, 1998: Statistical characteristics of a real-time precipitation forecasting model. *Wea. Forecasting,* **13,** 966–982.
Grabowski, W. W., 2001: Coupling cloud processes with the large-scale dynamics using the cloud-resolving convection parameterization (CRCP). *J. Atmos. Sci.,* **58,** 978–997.
Hallett, J., and S. C. Mossop, 1974: Production of secondary ice crystals during the riming process. *Nature,* **249,** 25–28.
Heggli, M. F., L. Vardiman, R. E. Stewart, and A. Huggins, 1983: Supercooled liquid water and ice crystal distributions within Sierra Nevada winter storms. *J. Appl. Meteor.,* **22,** 1875–1886.
Hobbs, P. V., 1978: Organization and structure of clouds and precipitation on the mesoscale and microscale in cyclonic storms. *Rev. Geophys. Space Phys.,* **16,** 741–755.
——, and A. L. Rangno, 1985: Ice particle concentrations in clouds. *J. Atmos. Sci.,* **42,** 2523–2549.
——, and ——, 1990: Rapid development of high ice particle concentrations in small polar maritime cumuliform clouds. *J. Atmos. Sci.,* **47,** 2710–2722.
——, L. F. Radke, A. B. Fraser, and R. R. Weiss, 1971: The Cascade Project: A study of winter cyclonic storms in the Pacific Northwest. *Proc. Int. Conf. on Weather Modification,* Canberra, Australia.
——, S. Chang, and J. D. Locatelli, 1974: The dimensions and aggregation of ice crystals in natural clouds. *J. Geophys. Res.,* **79,** 2199–2206.
——, T. J. Matejka, P. H. Herzegh, J. D. Locatelli, and R. A. Houze Jr., 1980: The mesoscale and microscale structure and organization of clouds and precipitation in midlatitude cyclones. I: A case study of a cold front. *J. Atmos. Sci.,* **37,** 568–596.
Hogg, D. C., F. O. Guiraud, J. B. Snider, M. T. Decker, and E. R. Westwater, 1983: A steerable dual-channel microwave radiometer for measurement of water vapor and liquid in the troposphere. *J. Appl. Meteor.,* **22,** 789–806.
Houze, R. A., Jr., S. A. Rutledge, T. J. Matejka, and P. V. Hobbs, 1981: The mesoscale and microscale structure and organization of clouds and precipitation in midlatitude cyclones. III: Air motions and precipitation growth in a warm-frontal rainband. *J. Atmos. Sci.,* **38,** 639–649.
Kessler, E., 1969: *On the Distribution and Continuity of Water Substance in Atmospheric Circulations. Meteor. Monogr.,* No. 32, Amer. Meteor. Soc., 84 pp.

Khairoutdinov, M., and Y. Kogan, 2000: A new cloud physics parameterization in a large-eddy simulation mode of marine stratocumulus. *Mon. Wea. Rev.,* **128,** 229–243.

——, and D. A. Randall, 2001: A cloud-resolving model as a cloud parameterization in the NCAR Community Climate System model: Preliminary results. *Geophys. Res. Lett.,* **28,** 3617–3620.

Khvorostyanov, V. I., and J. A. Curry, 2002: Terminal velocities of droplets and crystals: Power laws with continuous parameters over the size spectrum. *J. Atmos. Sci.,* **59,** 1872–1884.

Lawson, R. P., and T. L. Jensen, 1998: Improved microphysical observations in mixed phase clouds. Preprints, *Conf. on Cloud Physics,* Everett, WA, Amer. Meteor. Soc., 451–454.

——, R. E. Stewart, J. W. Strapp, and G. A. Isaac, 1993: Aircraft observations of the origin and growth of very large snowflakes. *Geophys. Res. Lett.,* **20,** 53–56.

——, ——, and L. J. Angus, 1998: Observations and numerical simulations of the origin and development of very large snowflakes. *J. Atmos. Sci.,* **55,** 3209–3229.

Lin, Y.-L., R. D. Farley, and H. D. Orville, 1983: Bulk parameterization of the snow field in a cloud model. *J. Climate Appl. Meteor.,* **22,** 1065–1092.

Locatelli, J. D., and P. V. Hobbs, 1974: Fall speeds and masses of solid precipitation particles. *J. Geophys. Res.,* **79,** 2185–2197.

Manning, K. W., and C. A. Davis, 1997: Verification and sensitivity experiments for the WISP94 MM5 forecasts. *Wea. Forecasting,* **12,** 719–735.

Manton, M. J., and W. R. Cotton, 1977: Parameterization of the atmospheric surface layer. *J. Atmos. Sci.,* **34,** 331–334.

Mass, C. F., D. Ovens, K. Westrick, and B. A. Colle, 2002: Does increasing horizontal resolution produce more skillful forecasts? *Bull. Amer. Meteor. Soc.,* **83,** 407–430.

Meyers, M. P., P. J. DeMott, and W. R. Cotton, 1992: New primary ice-nucleation parameterizations in an explicit cloud model. *J. Appl. Meteor.,* **31,** 708–721.

——, R. L. Walko, J. Y. Harrington, and W. R. Cotton, 1997: New RAMS cloud microphysics parameterization. Part II: The two-moment scheme. *Atmos. Res.,* **45,** 3–39.

Mitchell, D. L., 1996: Use of mass- and area-dimensional power laws for determining precipitation particle terminal velocities. *J. Atmos. Sci.,* **53,** 1710–1723.

Mossop, S. C., 1985: The microphysical properties of supercooled cumulus clouds in which an ice particle multiplication process operated. *Quart. J. Roy. Meteor. Soc.,* **111,** 183–198.

Olson, D. A., N. W. Junker, and B. Korty, 1995: Evaluation of 33 years of quantitative precipitation forecasting at the NMC. *Wea. Forecasting,* **10,** 498–511.

Rangno, A. L., and P. V. Hobbs, 1991: Ice particle concentrations and precipitation development in small polar maritime cumuliform clouds. *Quart. J. Roy. Meteor. Soc.,* **117,** 207–241.

——, and ——, 1994: Ice particle concentrations and precipitation development in small continental cumuliform clouds. *Quart. J. Roy. Meteor. Soc.,* **120,** 573–601.

Rasmussen, R., and Coauthors, 1992: Winter Icing and Storms Project (WISP). *Bull. Amer. Meteor. Soc.,* **73,** 951–974.

——, J. Vivekanandan, J. Cole, B. Myers, and C. Masters, 1999: The estimation of snowfall rate using visibility. *J. Appl. Meteor.,* **38,** 1542–1563.

——, I. Geresdi, G. Thompson, K. Manning, and E. Karplus, 2002: Freezing drizzle formation in stably stratified layer clouds: The role of radiative cooling of cloud dropets, cloud condensation nuclei, and ice initiation. *J. Atmos. Sci.,* **59,** 837–860.

Reinking, R. F., J. B. Snider, and J. L. Coen, 2000: Influences of storm-embedded orographic gravity waves on cloud liquid water and precipitation. *J. Appl. Meteor.,* **39,** 733–759.

Reisner, J., R. M. Rasmussen, and R. T. Bruintjes, 1998: Explicit forecasting of supercooled liquid water in winter storms using the MM5 mesoscale models. *Quart. J. Roy. Meteor. Soc.,* **124,** 1071–1107.

Reynolds, D. W., and A. S. Dennis, 1986: Review of the Sierra Cooperative Pilot Project. *Bull. Amer. Meteor. Soc.,* **67,** 513–523.

Rutledge, S. A., and P. V. Hobbs, 1983: The mesoscale and microscale structure and organization of clouds and precipitation in midlatitude cyclones. VIII. A model for the "seeder-feeder" process in warm-frontal rainbands. *J. Atmos. Sci.,* **40,** 1185–1206.

——, and ——, 1984: The mesoscale and microscale structure and organization of clouds and precipitation in midlatitude cyclones. XII: A diagnostic modeling study of precipitation development in narrow cold-frontal rainbands. *J. Atmos. Sci.,* **41,** 2949–2972.

Straka, J. M., and E. N. Rasmussen, 1997: Toward improving microphysical parameterizations of conversion processes. *J. Appl. Meteor.,* **36,** 896–902.

Telford, J. W., 1988: An example of the behavior of an aircraft with accumulated ice: Latent instability. *J. Appl. Meteor.,* **27,** 1093–1108.

——, and P. B. Wagner, 1981: Observations of condensation growth determined by entity type mixing. *Pure Appl. Geophys.,* **119,** 934–965.

Vivekanandan, J., D. S. Zrni , S. M. Ellis, R. Oye, A. V. Ryzhkov, and J. Straka, 1999: Cloud microphysics retrieval using S-band dual-polarization radar measurements. *Bull. Amer. Meteor. Soc.,* **80,** 381–388.

Westrick, K. J., and C. F. Mass, 2001: An evaluation of a high-resolution hydrometeorological modeling system for prediction of a cool-season flood event in a coastal mountainous watershed. *J. Hydrometeor.,* **2,** 161–180.

White, A. B., J. R. Jordan, B. E. Martner, F. M. Ralph, and B. W. Bartram, 2000: Extending the dynamic range of an S-band radar for cloud and precipitation studies. *J. Atmos. Oceanic Technol.,* **17,** 1226–1234.

Wurman, J., 1994: Vector winds from a single-transmitter bistatic dual-Doppler radar network. *Bull. Amer. Meteor. Soc.,* **75,** 983–994.

——, S. Heckman, and D. Boccippio, 1993: A bistatic multiple-Doppler network. *J. Appl. Meteor.,* **32,** 1802–1814.

Zikmunda, J., and G. Vali, 1972: Fall patterns and fall velocities of rimed ice crystals. *J. Atmos. Sci.,* **29,** 1334–1347.